CORONAVIRUS

Abrupt but smaller than expected changes in surface air quality attributable to COVID-19 lockdowns

Zongbo Shi[1]*[†], Congbo Song[1]*[†], Bowen Liu[2], Gongda Lu[1], Jingsha Xu[1], Tuan Van Vu[3], Robert J. R. Elliott[2], Weijun Li[4], William J. Bloss[1], Roy M. Harrison[1]‡

The COVID-19 lockdowns led to major reductions in air pollutant emissions. Here, we quantitatively evaluate changes in ambient NO_2, O_3, and $PM_{2.5}$ concentrations arising from these emission changes in 11 cities globally by applying a deweathering machine learning technique. Sudden decreases in deweathered NO_2 concentrations and increases in O_3 were observed in almost all cities. However, the decline in NO_2 concentrations attributable to the lockdowns was not as large as expected, at reductions of 10 to 50%. Accordingly, O_3 increased by 2 to 30% (except for London), the total gaseous oxidant ($O_x = NO_2 + O_3$) showed limited change, and $PM_{2.5}$ concentrations decreased in most cities studied but increased in London and Paris. Our results demonstrate the need for a sophisticated analysis to quantify air quality impacts of interventions and indicate that true air quality improvements were notably more limited than some earlier reports or observational data suggested.

INTRODUCTION

Air pollution (both indoor and outdoor) is the single largest environmental risk to human health globally, contributing to 8.8 million deaths in 2015 (*1*). The World Bank estimated that air pollution costs the global economy $3 trillion in 2015 (*2*). It has been suggested that poor air quality is correlated with a higher mortality rate from COVID-19 infection (*3*). Although a causal relationship between the two is difficult to confirm, air pollution contributes to respiratory and cardiovascular diseases and thus has the potential to cause increased COVID-19 death rates (*4*).

In response to the COVID-19 crisis, governments around the world introduced severe restrictions on behavior or lockdowns, which led to the cessation of a large swathe of economic activity and thus reduced air pollutant emissions (*5*). The rapid and unprecedented reduction in the economic activity provides a unique opportunity to study the impact of a global-scale natural intervention on air pollution, which offers insights for the prioritization of future clean air actions.

Many recent studies have explored impacts of the COVID-19 lockdowns on air quality. The most common approach is to undertake a simple statistical analysis that compares air quality before and after the lockdowns began or during the lockdowns with the same periods in previous years (*6*, *7*). Some studies also compared the air quality before and after lockdown started for periods with similar meteorological conditions (*8*). Satellite observations of NO_2 have also been used to estimate the reduction in column NO_2 due to the lockdowns (*3*, *9*–*11*).

A major caveat in a number of these studies is that meteorology moderates the link between emissions and pollutant concentrations, and so, weather changes can mask the changes in emissions on air quality (*12*–*14*). Such methods cannot explain the observed severe pollution events during the lockdowns in some cities (*15*–*17*). Comparisons of pollutant levels in 2020 with previous years may assume that air pollutant emissions have not changed over the past few years, which is often not the case, particularly in those cities where clean air policy actions are in place (*14*, *18*). Furthermore, air pollutant emissions change substantially from winter to spring; thus, a direct comparison of air pollutant concentrations before and during the lockdowns could also give unreliable results. Venter *et al.* (*9*) developed statistical models (regression) to estimate the impact of lockdowns on air quality in several countries. However, the performance of the regression was often limited with correlation coefficients as low as 0.2. He *et al.* (*19*) applied a "difference-in-difference" approach, which may provide a more accurate estimate of air quality improvement; this method assumes that the control cities are not subject to any impacts.

Air quality modeling can also decouple the effect of emission changes from meteorology (*20*, *21*) and is often applied for scenario analysis. A major challenge in evaluating the impacts of short-term interventions on real-world air quality is to estimate emission changes (*16*, *20*, *21*).

Machine learning offers an alternative and reliable method in quantifying changes in air quality due to emissions and meteorological factors (*12*–*14*). Myllyvirta and Thieriot (*22*) used a random forest (RF) method (*13*), which was developed for assessing long-term air quality changes, to estimate the short-term changes in NO_2 and PM_{10} in Europe due to the COVID-19 lockdowns (see Materials and Methods).

The purpose of this study was to evaluate the impacts and implications of the natural experiment of the COVID-19 lockdowns in spring 2020 on air quality. To do this, we optimized a weather normalization technique based on Grange and Carslaw (*13*) and Vu et al. (*14*) to decouple the effects of meteorology from short-term emission changes on surface air quality monitoring data in 11 global cities that were subjected to extensive lockdown measures. The deweathered data allow us to quantitatively evaluate the real-world changes in air quality due to the lockdown measures in these cities (see Materials and Methods). These selected cities cover a range of air pollution climates, from highly to less polluted and from $PM_{2.5}$- to NO_2-dominated

[1]School of Geography Earth and Environment Sciences, University of Birmingham, Birmingham B15 2TT, UK. [2]Department of Economics, University of Birmingham, Birmingham B15 2TT, UK. [3]School of Public Health, Imperial College London, London W2 1PG, UK. [4]Department of Atmospheric Sciences, School of Earth Sciences, Zhejiang University, Hangzhou 310027, China.
*These authors contributed equally to this work.
†Corresponding author. Email: z.shi@bham.ac.uk (Z.S.); c.song.1@bham.ac.uk (C.S.)
‡Also at: Department of Environmental Sciences and Center of Excellence in Environmental Studies, King Abdulaziz University, P.O. Box 80203, Jeddah 21589, Saudi Arabia.

pollution. Data were divided into roadside, urban background, and rural sites to better understand the impacts of road traffic and urban emissions on air quality changes.

RESULTS

We first estimated the percentage change (P) in the observed or deweathered concentrations of air pollutants using the following equation

$$P = \overline{(C_i - C)/C \times 100\%} \tag{1}$$

where C is the average concentration in the second and third weeks before the lockdown date or equivalent (as a prelockdown baseline), and C_i is the average concentrations in the ith day (from the 1st to 28th day) starting in the second week after the lockdown start date for each city and for each year (see Fig. 1). For example

$$P_{2020} = \overline{(C_{i,2020} - C_{2020})/C_{2020} \times 100\%} \tag{2}$$

The week immediately before and after the lockdown date was considered a transition period and so was excluded in the calculations. We recognize that the transition may have started earlier in some cities such as London, but for consistency, we applied the same Eq. 1 for calculation. For clarification, we will use P_{obs} and P_{dew} to represent changes in observed and deweathered concentrations, respectively.

We then estimated the detrended percentage change (P^*) in the concentration of each air pollutant (deweathered only; Fig. 1), calculated by

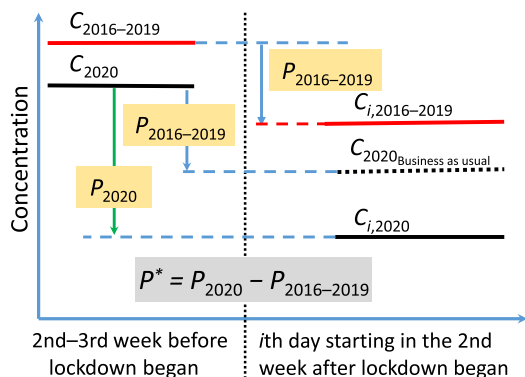$$P^* = P_{2020} - P_{2016-2019} \tag{3}$$

Fig. 1. Concept of detrending air pollutant levels. $C_{2016-2019}$ and C_{2020} are the average concentrations of an air pollutant in the second and third weeks before the lockdown start date or equivalent in 2016–2019 and 2020, respectively; $C_{i,2016-2019}$ and $C_{i,2020}$ are the daily average concentrations of an air pollutant in the ith day starting in the second week after the lockdown start date or equivalent in 2016–2019 and 2020, respectively. The vertical dashed line represents lockdown start date. $P_{2016-2019}$ and P_{2020} are the percentage changes in air pollutant levels after versus before the lockdown began or equivalent in 2016–2019 and 2020, respectively (see Eq. 2 in the main text for definition). $C_{2020\text{Business as usual}}$ is the hypothetical concentration for the ith day starting in the second week after the lockdown date under "business-as-usual" (i.e., no lockdown) conditions. This is calculated from the prelockdown concentration (C_{2020}) assuming the same percentage change as in 2016–2019 ($P_{2016-2019}$, as the "business-as-usual" change). The detrended percentage change P^* (i.e., the change in air pollutant concentration arising from lockdown effects alone) is given by $P_{2020} - P_{2016-2019}$.

where P_{2020} and $P_{2016-2019}$ are percentage changes in deweathered concentrations of air pollutants in 2020 and 2016–2019, respectively. P^* was calculated by Monte Carlo simulations ($n = 10,000$) based on the normal distribution of P_{2020} and $P_{2016-2019}$.

P^* removes the "business-as-usual" variability in concentrations from winter to spring (i.e., 2016–2019 as a baseline, $P_{2016-2019}$) and thus represents the change attributable to lockdown measures. This business-as-usual variability can be caused by changes in anthropogenic activities (e.g., domestic heating) and natural processes [e.g., biogenic volatile organic compound (VOC) emissions]. For example, when the domestic heating demand reduces in local spring, there may be less local emissions of air pollutants; as a result, the concentrations of air pollutants are lower if emissions from other major sources do not increase and meteorological conditions are similar.

Changes in NO₂, O₃, and Oₓ

Observed NO_2 levels are highly variable, with daily concentrations changing notably during the study period (Fig. 2 and fig. S1). Pollution events (e.g., spikes in Fig. 2) appeared repeatedly during the lockdowns, such as in Beijing, Wuhan, and Paris. Observed NO_2 at roadside sites decreased substantially in all cities after the lockdowns began, with P_{obs} ranging from −29.3 ± 33.1% in Berlin to −53.5 ± 18.9% in London (table S1); observed NO_2 at urban background sites also decreased substantially, with the P_{obs} ranging from −10.1 ± 36.6% in London to −60.2 ± 14.8% in Delhi; and observed NO_2 at rural sites increased in London (P_{obs} = +115.8 ± 90.2%) and Paris (P_{obs} = +99.2 ± 66.7%) but decreased in other cities after lockdown started.

Deweathered NO_2 usually shows a similar pattern to the observations, but the magnitudes and sometimes even the signs of changes are different. A sudden drop, distinct from the data in 2018, is clearly observed at urban sites in 2020 after the lockdowns began in all cities except London and Los Angeles, which show a more gradual change (Fig. 2 and fig. S1). This confirms that the sudden changes in 2020 are indeed due to the lockdown measures.

Deweathered NO_2 at urban background sites in 2020 decreased in all cities after the lockdowns began, with P_{dew} ranging from −18.2 ± 6.0% in London to −52.9 ± 1.4% in Delhi (Table 1); deweathered NO_2 at roadside sites decreased more markedly in most cities (Fig. 2, fig. S1, and table S2). We also noticed that deweathered NO_2 (P_{dew}) in 2016–2019 decreased in almost all cities from winter to spring, although the magnitude of change is usually much smaller than in 2020 (Fig. 3). Thus, the absolute values of the detrended NO_2 change, P^*, is smaller than the corresponding P_{dew}. Table 1 shows that the decline in NO_2 due to the lockdown measures at urban background sites is mostly less than 30% in the studied cites.

Deweathered NO and NO_x (=NO + NO_2) in 2020 dropped more markedly (table S2) after the lockdown began than was observed for NO_2. For example, P_{dew} values for NO and NO_x at urban background sites in London were approximately −24.8 ± 6.3 and −21.0 ± 5.9%, respectively, whereas that for NO_2 was −18.2 ± 6.0%. At roadside sites in London and Rome, deweathered NO_x decreased by more than 50% during the lockdowns, a much larger change than that for NO_2 (−47.0% in London and −35.2% in Rome).

In contrast to changes in NO_2, observed O_3 at roadside sites in 2020 increased in all cases (fig. S1 and table S1) after the lockdown began, with the P_{obs} values ranging from +19.5 ± 21.0% in Madrid to +155.6 ± 83.2% in Milan. Observed O_3 at urban/rural sites also increased during the lockdowns (fig. S1). A sudden increase in
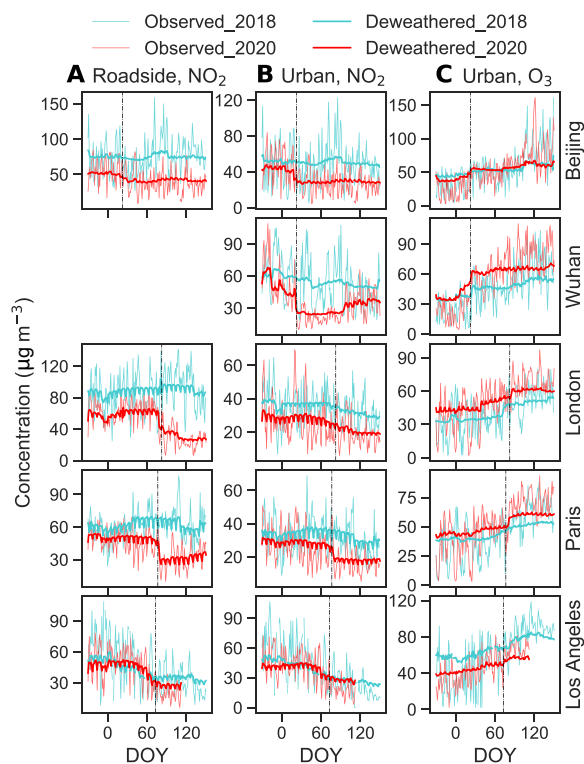
Fig. 2. Observed and deweathered daily NO₂ and O₃ concentrations in selected cities before and after the lockdown start dates or equivalent in 2020 versus 2018. Columns correspond to (**A**) NO_2 at roadside sites, (**B**) NO_2 at urban background sites, and (**C**) O_3 at urban background sites; rows show different cities as indicated. Fine and heavy lines indicate observed and deweathered concentrations, respectively. Data are shown from December to May, shown as day of year (DOY; 1 January = 1), where the vertical dashed lines represent lockdown date. The sudden drop in deweathered NO_2 and corresponding increase in deweathered O_3 are apparent in Beijing, Wuhan, and Paris, whereas London and Los Angeles show more gradual changes. The saw-like shape in the deweathered data in some cities captures the weekly cycles of NO_2 and, to a lesser extent, O_3, particularly in western cities. Results from other cities/sites are shown in fig. S1. No data are available for roadside sites in Wuhan.

deweathered O_3 after the lockdown began was observed in most of the cities (Fig. 1 and fig. S1). The P_{dew} values (Table 1 and table S2) for deweathered O_3 range from +15.0 ± 3.0% in Los Angeles to +128.5 ± 41.9% in Milan at roadside sites, from +14.8 ± 2.2% in Los Angeles to +66.8 ± 29.2% in Milan at urban background sites, and from +1.5 ± 0.9% in London to +57.9 ± 6.3% in Milan at rural sites. However, there is an increasing trend in O_3 levels at urban background sites during the same periods in 2016–2019 (Figs. 2 and 3), with P_{dew} values ranging from +12.1 ± 9.1% in New York to +51.2 ± 23.4% in Milan (auxiliary data table S1). As a result, the detrended O_3 changes (P^*) at urban background sites are much smaller than those of the corresponding P_{dew} values; there is an obvious increase in P^* in Beijing, Wuhan, Milan, and Rome, but a small change or even a decrease in other cities (Table 1).

Accordingly, the observed levels of total gaseous oxidant (i.e., $O_x = NO_2 + O_3$), a parameter unaffected by the titration reaction between NO and O_3 but representing net photochemical production of O_3, showed a different pattern to NO_2 and O_3, with little change before and during the lockdowns, whether at roadside, urban background, or rural sites (Fig. 4). Observed O_x at urban background

sites in 2020 range from 35.0 ± 5.4 parts per billion (ppb) in Madrid to 44.8 ± 8.5 ppb in Delhi during the 10-week period with lockdown start date in the middle. Deweathered O_x mixing ratios at urban background sites were remarkably similar across the cities, at approximately 40 ppb (Fig. 4). Only a small change in deweathered O_x, before and after lockdown started in 2020, was observed at urban background sites in all the cities, with P_{dew} values ranging from −4.6 ± 3.5% in Delhi to +10.5 ± 0.8% in Berlin (Table 1). Small changes were also seen during the same periods in 2016–2019, with P_{dew} for deweathered O_3 ranging from −1.2 ± 7.1% in Beijing to +8.7 ± 1.7% in Berlin (Fig. 2 and auxiliary data table S1). Detrended O_x at urban background sites generally decreased during the study period in most of the cities, but the absolute change is relatively small, i.e., mostly within ±5%; changes at rural sites are more variable with almost half of the cities showing a slight increase (table S3).

Changes in PM₂.₅ and PM₁₀
Figure 5 and fig. S2 show that the average observed $PM_{2.5}$ levels in 2020 reduced after lockdown started in the two more polluted cities, Wuhan and Delhi. No clear changes were observed in other cities, particularly when comparing levels to those in previous years (Fig. 5 and fig. S2). In Beijing, Paris, and London, pollution events were observed after the lockdowns began (Fig. 5). Unlike NO_2, the peak levels observed during the lockdowns were sometimes even higher than those before lockdown began (e.g., London). The P_{obs} values for observed $PM_{2.5}$ in 2020 range from −40.8 ± 28.4% in Los Angeles to +107.6 ± 148.5% in London at roadside sites, from −38.6 ± 17.2% in Madrid to +152.9 ± 165.0% in London at urban background sites, and from −34.2 ± 26.8% in Delhi to +164.5 ± 148.7% in London at rural sites (table S1).

Deweathered $PM_{2.5}$ in 2020 showed a clearer pattern than that apparent in the observations (Fig. 5). Unlike deweathered NO_2 and O_3, a sudden decrease in $PM_{2.5}$ after lockdowns started was not detected in most of the cities, with the exceptions of Wuhan and Rome (fig. S1). However, sudden decreases were observed in some cities (such as Los Angeles, New York, Beijing, and Wuhan) a few days after or before the lockdowns began. Figure 5 and fig. S2 show that the deweathered $PM_{2.5}$ before the lockdown began in 2020 was similar to that in 2018 in Beijing, lower in Wuhan, London, Paris, and Berlin, but higher in Rome and Delhi. In Beijing, there was an increase in deweathered $PM_{2.5}$ after the lockdown began initially, but there was a decrease afterward (Fig. 5). Deweathered $PM_{2.5}$ in London and Paris also increased after the lockdowns began, but in contrast, there was no obvious decrease even 3 weeks from the lockdown date.

The changes in deweathered $PM_{2.5}$ are similar at different site types (Fig. 5 and fig. S2). Deweathered $PM_{2.5}$ at roadside sites in 2020 increased slightly during the lockdowns by +1.0 ± 7.2% in London and +0.2 ± 9.1% (P_{dew}) in Paris but decreased with changes (P_{dew}) ranging from −2.8 ± 1.3% in New York to −37.8 ± 4.8% in Los Angeles (table S2). A similar trend is also observed in the deweathered $PM_{2.5}$ at urban background and rural sites (Fig. 5 and fig. S2). An obvious decrease in deweathered $PM_{2.5}$ at urban background sites during the same study periods was also observed in 2016–2019 in some cities but not in others (Fig. 3 and auxiliary data table S1). The detrended change (P^*; Table 1) in $PM_{2.5}$ at urban background sites shows a decrease in Los Angeles (−40.3 ± 26.9%), Madrid (−24.1 ± 18.4%), Wuhan (−15.7 ± 24.8%), New York (−13.9 ± 6.9%), and Delhi (−5.2 ± 4.8%), but little changes or even increases in the other cities.

Table 1. Percentage changes (%) in deweathered (P_{dew}) and detrended (P^*) NO$_2$, O$_3$, PM$_{2.5}$ mass concentrations, and O$_x$ mixing ratios at urban background sites in the studied cities. See Eqs. 1 to 3 for definition of P_{dew} and P^*. N.A., data not available.

		Beijing	Wuhan	Milan	Rome	Madrid	London	Paris	Berlin	New York	Los Angeles	Delhi
NO$_2$	P_{dew}	−33.4 ± 2.2	−43.9 ± 2.2	−27.4 ± 8.3	−33.2 ± 6.1	−49.7 ± 3.1	−18.2 ± 6.0	−33.6 ± 3.3	−25.4 ± 6.0	−23.3 ± 2.0	−23.8 ± 3.4	−52.9 ± 1.4
	P^*	−18.5 ± 9.2	−33.9 ± 7.3	−16.3 ± 11.4	−27.1 ± 7.7	−35.2 ± 21.3	−7.7 ± 7.7	−25.8 ± 7.1	−11.3 ± 13.1	−17.0 ± 8.3	−9.9 ± 6.1	−51.0 ± 5.2
O$_3$	P_{dew}	28.9 ± 2.0	44.5 ± 3.4	66.8 ± 29.2	55.8 ± 6.7	28.0 ± 3.8	15.8 ± 1.8	22.2 ± 2.4	29.9 ± 3.0	17.4 ± 3.9	14.8 ± 2.2	26.2 ± 5.8
	P^*	14.8 ± 5.3	21.8 ± 13.6	15.4 ± 37.6	29.8 ± 10.1	11.2 ± 18.3	−1.6 ± 8.1	7.0 ± 5.1	2.6 ± 8.9	5.3 ± 9.8	2.3 ± 5.3	8.2 ± 8.4
PM$_{2.5}$	P_{dew}	−19.3 ± 9.6	−27.0 ± 18.7	N.A.	−16.4 ± 5.2	−43.1 ± 3.4	8.6 ± 8.3	16.5 ± 10.7	N.A.	−21.5 ± 2.6	−18.0 ± 5.4	−12.7 ± 2.8
	P^*	−2.4 ± 14.7	−15.7 ± 24.8	N.A.	−0.7 ± 9.6	−24.1 ± 18.4	10.9 ± 16.7	27.4 ± 15.3	N.A.	−13.9 ± 6.9	−40.3 ± 26.9	−5.2 ± 4.8
O$_x$	P_{dew}	−1.1 ± 2.0	1.1 ± 1.4	−1.3 ± 1.0	4.1 ± 1.2	−0.4 ± 1.3	4.2 ± 0.8	2.1 ± 0.6	10.5 ± 0.8	−1.0 ± 1.8	−2.3 ± 1.0	−4.6 ± 3.5
	P^*	0.1 ± 7.4	−0.7 ± 4.4	−7.2 ± 5.9	−2.0 ± 2.9	−3.4 ± 3.2	−2.4 ± 1.3	−0.6 ± 2.3	1.8 ± 1.9	−6.4 ± 6.8	−4.1 ± 1.7	−9.8 ± 6.3
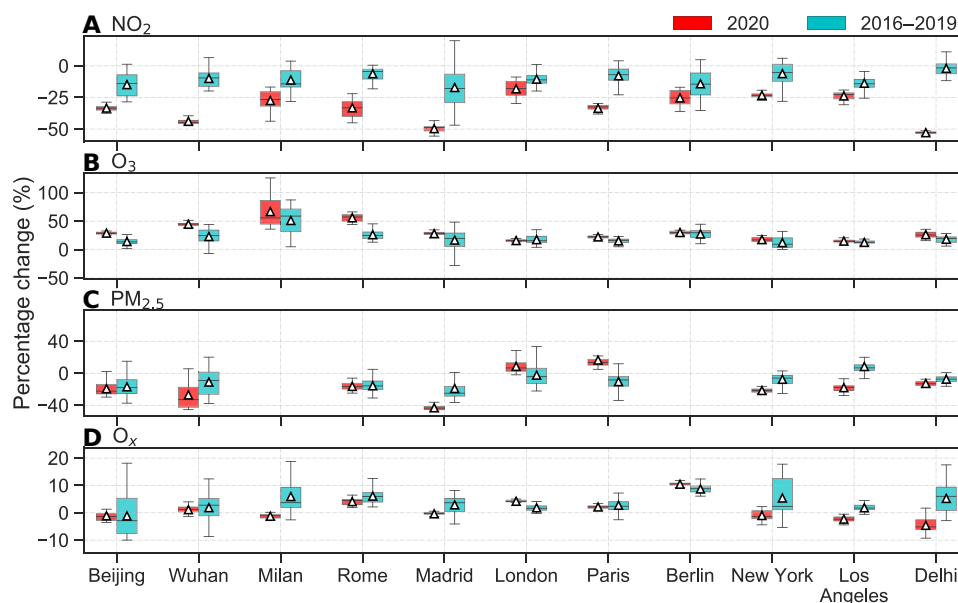
Fig. 3. Box plots of percentage change (P_{dew}) in deweathered concentrations of air pollutants in 2020 versus 2016–2019. Rows represent (**A**) NO$_2$, (**B**) O$_3$, (**C**) PM$_{2.5}$, and (**D**) O$_x$. Lower and upper box boundaries represent the 25th and 75th percentiles, respectively; line and triangle inside boxes represent median and mean values, respectively; lower and upper error lines represent 1.5 * IQR (interquartile range) below the third quartile and above the first quartile, respectively. Number of samples for P_{dew} in 2020 and 2016–2019 is usually 28 and 112, respectively.

The overall patterns of variations in observed and deweathered PM$_{10}$ (fig. S4) are similar to those of the PM$_{2.5}$ (fig. S3). A slight difference in some cities is that there were more variabilities/contrasting patterns at different types of site. For example, a larger decline in P_{dew} for deweathered PM$_{10}$ at roadside sites than that at urban background sites is observed in Beijing, Madrid, London, Paris, and Berlin (table S2), potentially reflecting a coarse particle source from road traffic (e.g., non–exhaust emissions) (23). Furthermore, in Los Angeles and Delhi, the decline in deweathered PM$_{10}$ is significantly larger than that of PM$_{2.5}$ whether at urban background or rural sites (table S2), implying a reduced contribution of coarse particles to PM$_{10}$.

Changes in CO and SO$_2$
Deweathered CO levels were lower after lockdown started than before in 2020. This pattern is different from that in 2018 (fig. S4). A sudden change is observed in Rome and Wuhan only. In Beijing,

deweathered CO increased slightly after the lockdown began, before falling for about 2 weeks, after which there was a substantial increase at all three types of sites. Thereafter, the deweathered CO decreased substantially, ~40% (P_{dew}) lower than that during the same period in 2018. In New York (roadside sites), a decline in deweathered CO is observed a week after the lockdown began. In Delhi, the decreasing trend in deweathered CO at urban background sites is not distinguishable from that in 2018, whereas at rural sites, CO clearly declined from a few days before the lockdown began.

The change in deweathered SO$_2$ after the lockdowns began is dependent on the site or city (fig. S4). No sudden change is observed in any of the cities immediately after the lockdowns. In Beijing, deweathered roadside and urban SO$_2$ increased initially and then decreased by ~20%. In all cases, the deweathered SO$_2$ concentration in 2020 is much lower than that in 2018. In London, deweathered SO$_2$ declined for a few days before the lockdown began at roadside sites. Deweathered SO$_2$ in Wuhan and Rome decreased about a month
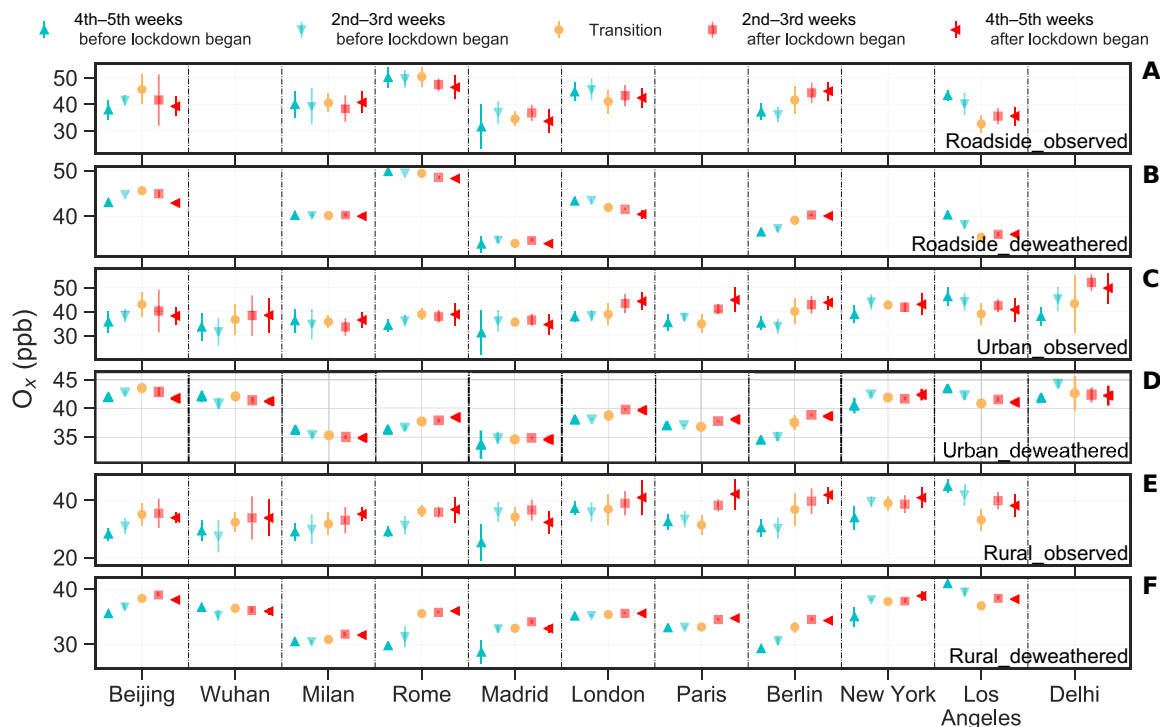
Fig. 4. Observed and deweathered O_x (i.e., $NO_2 + O_3$) mixing ratios in the 5 weeks before and after the lockdown start dates in the studied cities in 2020. The six rows (from top to bottom) show results from roadside observed (**A**) and deweathered (**B**), urban background observed (**C**) and deweathered (**D**), and rural observed (**E**) and deweathered (**F**) mixing ratios. Deweathered O_x shows little change before and after the lockdown dates in 2020 and is similar across all urban background sites (all close to 40 ppb). Error bars (included for all points) represent 1 SD ($n = 14$). Transition period refers to the 2 weeks with the lockdown start date in the middle.

before the lockdowns but did not change during the lockdowns. In New York (roadside sites), a decline in deweathered SO_2 is observed a week after the lockdown began. Delhi saw a substantial decrease in deweathered SO_2 about 2 weeks after the lockdown started, and the decrease in deweathered CO at urban background sites is not distinguishable from that in 2018, whereas at rural sites, it clearly declined from a few days before the lockdown began.

DISCUSSION
The deweathered and detrended data are used to understand how the air quality responded to the changes in activity associated with the COVID-19 lockdowns of early 2020 and the potential implications of such interventions for developing future air pollution abatement strategies and thus improving human health.

The importance of deweathering and detrending
Large differences between the deweathered and observed concentrations of air pollutants were observed in the studied cities (Fig. 2 and figs. S1 to S3). Observed daily average NO_2 concentrations are much higher than the deweathered ones during some periods. Our estimated NO_2 decline in Wuhan due to lockdown effects is much lower than that estimated by Le *et al.* (*15*), who reported up to 93% reduction in NO_2 in Wuhan during the lockdown. If we look at the observations only, we can indeed see >90% decrease from the peak concentration before the lockdown began to the lowest one afterward (Fig. 2), but this is mainly due to changes in meteorological conditions, not emissions. The observed $PM_{2.5}$ also exhibited

remarkable meteorologically driven variability regardless of cities or site types and sometimes differed by more than a factor of 3 when compared with deweathered concentrations (Fig. 5 and fig. S2). In general, major differences are apparent between the observed and deweathered results when the meteorological conditions change substantially over the study period. For example, the changes in observed and deweathered $PM_{2.5}$ at urban background sites in Beijing before and after the lockdown began were $+19.2 \pm 108.6\%$ (P_{obs}) and $-19.3 \pm 9.6\%$ (P_{dew}), respectively. In this case, emission reductions and the unfavorable meteorological conditions drove changes of approximately -19.3 and $+38.6\%$ in the observed levels, respectively, leading to an overall $+19.2\%$ increase in $PM_{2.5}$. Our results demonstrate that meteorological variations, rather than emission changes on the scale of those occurring during the COVID-19 lockdowns, dominate short-term variability in air pollutant concentrations, which is consistent with previous studies (*12*, *14*, *20*, *24*).

Apart from deweathering, detrending the "business-as-usual" changes is also crucial in estimating real changes attributable to interventions (i.e., lockdowns). In the "business-as-usual" scenario, air pollutant emissions (both anthropogenic and natural) and, thereby, concentrations may change from winter to spring, whether there is a lockdown or not (see 2016–2019 data in Fig. 3). For example, a general increase in deweathered O_3 is observed from winter to spring in 2016–2019 in all the studied cities (Figs. 2 and 3 and fig. S1). Such an increase reflects changing photochemical steady-state partitioning from NO_2 to O_3 (Northern Hemisphere cities moving into spring with increased solar radiation intensity and day length),
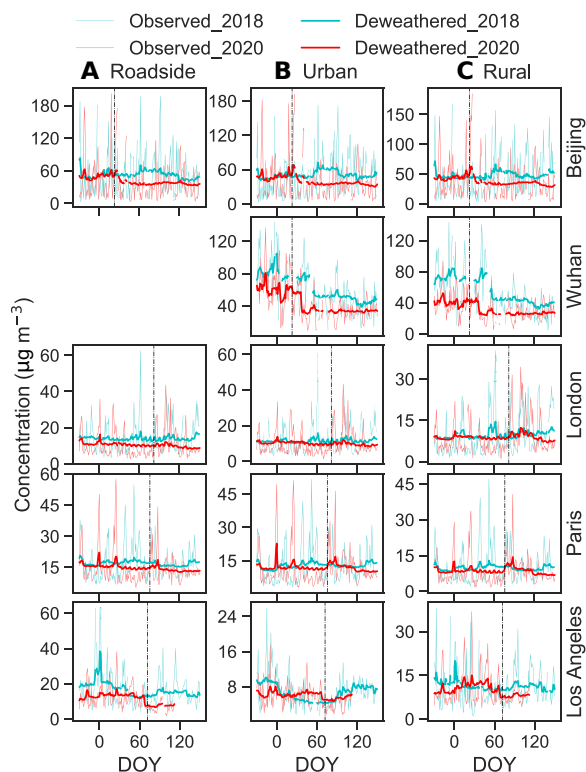
Fig. 5. Observed and deweathered daily PM$_{2.5}$ concentrations in the selected cities before and after the lockdown start dates or equivalent in 2020 versus 2018. Columns correspond to (**A**) roadside, (**B**) urban background, and (**C**) rural sites; rows show different cities as indicated. Fine and heavy lines indicate observed and deweathered concentrations, respectively. Data are shown from December to May, shown as day of year (1 January = 1), where the vertical dashed lines represent lockdown start date. Results from other cities/sites are shown in fig. S2. No data are available for roadside sites in Wuhan.

alongside wider increases in photochemical ozone formation, enhanced by increased emission and chemical reactivity of VOCs. Taking this "business-as-usual" variability into account, the detrended percentage changes (P^*) in O$_3$ are much smaller than the corresponding P_{dew} (Table 1 and table S3). Not accounting for this seasonality would lead to a different conclusion, as by Sicard *et al.* (*7*), that O$_3$ concentration increased substantially in response to the lockdowns.

In some cities, there are considerable variabilities in P_{dew} in 2016–2019 (Fig. 3). This may be partly due to specific events such as holidays around the lockdown dates, leading to a decrease in air pollutant emissions for a particular year. In this instance, the absolute value of P_{dew} in 2016–2019 could be slightly overestimated, and thus that of the P^* underestimated. However, because we included 4 years of data (2016–2019) for detrending, the impact of a specific event on the P^* values is small.

Our detrended results (Table 1 and table S3) demonstrate that the decreases in NO$_2$ and increases in O$_3$ due to the COVID-19 lockdowns are not as large as previous studies have reported (*7*, *21*) or as the raw observational data show (table S1). Note also that anthropogenic air pollutant emissions reduce year by year, such as in London and Beijing, as a result of clean air policy actions and vehicle fleet evolution (*14*, *18*). Thus, the approach widely used in the literature to estimate the lockdown effects by subtracting NO$_2$ during the equivalent periods in earlier years from that in 2020 (*6*, *7*, *11*, *15*)

may also overestimate the effects attributed to the lockdowns (Fig. 3 and Table 1).

Considering urban background sites in Wuhan (a widely studied city) as an example, observed NO$_2$ and O$_3$ changed by −47.3 ± 17.4% and +166.5 ± 60.5% (P_{obs} values, obtained from unadjusted concentration data before/during lockdown; table S1), values similar to those reported by Shi and Brasseur [−54 ± 7% and + 220 ± 20% (*25*)]; changes of approximately −51.8 and +40.0% are obtained by subtracting NO$_2$ and O$_3$ concentrations during the second to fifth weeks after the lockdown dates in 2016–2019 from those in 2020 (i.e., without adjustment for meteorology), values which are similar to those reported by Sicard *et al.* [−57 and +36% (*7*)]. Our estimated changes in deweathered NO$_2$ and O$_3$ (P_{dew}) are −43.9 ± 2.2% and +44.5 ± 3.4%, which are similar to those reported by Zhao *et al.* [−51.7 and +58% (*21*)]. However, these estimations (*7*, *21*, *25*) are considerably higher (sometimes by a factor of 10) than our detrended results (P^*), which are −33.9 ± 7.3% for NO$_2$ and +21.8 ± 13.6% for O$_3$. This may at least partially explain why the estimated changes in NO$_2$ and O$_3$ due to the lockdown effects in the studied cities reported here are lower than those published elsewhere (*7*, *11*, *15*, *21*, *25*), and demonstrate the necessity of disentangling the changes due to meteorological variation and seasonality and from the lockdown-driven changes in emissions to understand the resulting differences in air pollutant concentrations.

Drivers of changes

The deweathered NO$_2$ showed a sudden decrease after the lockdown began in most of the cities (Fig. 2 and fig. S1). Detrended NO$_2$ at urban background sites declined the most in Delhi (−51.0 ± 5.2%), Madrid (−35.2 ± 21.3%), and Wuhan (−33.9 ± 7.3%) (Table 1). A given reduction in NO$_x$ emission, and hence NO$_x$ abundance, is expected to lead to a smaller reduction in ambient NO$_2$ levels, as the fast NO$_x$-O$_3$ photochemistry shifts the NO$_2$/NO$_x$ ratio in favor of NO$_2$. The fact that the NO$_x$ changes are larger than those of NO$_2$ supports this argument (tables S1 and S2). A substantially larger decline in NO$_x$ and NO$_2$ was observed at roadside than at urban background sites, suggesting that the decline in NO$_2$ during the lockdowns is largely driven by changes in road traffic as the dominant source of NO$_x$ in urban atmosphere (*16*). Mobility data from Google Maps (https://google.com/covid19/mobility/) suggest that traffic volumes reduced by 60 to 80% in the cities considered here. However, this mobility decrease does not correspond directly to the same reduction in road traffic–related NO$_x$ emissions. For example, in London, although private car use reduced by about 80%, heavy good vehicles (HGVs) on the road only reduced by 30 to 40%. It is possible that if the change in the number of HGVs, which account for a smaller percentage of total vehicle population but a large proportion of vehicular NO$_x$ emissions (*26*, *27*), is small, then the changes in total road traffic emissions of NO$_x$ may be much smaller than expected. Decreases in activity levels from other combustion sources, such as power plants and industry (*22*), may have contributed to the decline in NO$_2$, at least in some cities, as shown by the small decline in SO$_2$ in some cities (fig. S4). Such changes are difficult to quantify, but the much smaller (and absence of any sudden) changes in SO$_2$ compared with NO$_2$ (Fig. 2 and fig. S2)—as indicated by the increase in SO$_2$/NO$_2$ ratio in Wuhan, London, Paris, Rome, and Delhi (auxiliary data table S1)—suggest that reductions in NO$_x$ emissions from stationary sources were less than those from traffic emissions. This is consistent with Le Quéré *et al.* (*5*), who estimated

that in Europe and the United States, electricity use reduced by 9 and 5%, respectively. Note also that domestic emissions may have increased with an increase in people working or studying from home. We recognize that our methodology is unable to attribute the actual changes in emissions on a sector-by-sector basis. This could be revisited in the future when emission inventories for the spring 2020 lockdown period are developed and evaluated against observations.

O_3 is a secondary pollutant, and its variation is driven by several factors. Dominant among these is the NO_x-O_3 photochemical steady state. The decrease in NO (tables S1 and S2) led to reduced O_3 titration, through which reductions in traffic-related NO emissions translate directly into increases in O_3, relative to the prelockdown period; the time constant for this NO_x-O_3 interaction in daylight is of the order of minutes. The fact that deweathered O_3 increased suddenly after the lockdown began and that changes in deweathered NO were more pronounced than those in NO_x and NO_2, particularly at roadside sites (fig. S1 and table S2), support this well-understood atmospheric chemistry (28). This effect—of a reduced urban decrement in O_3—will be partially offset by reductions in primary NO_2 emissions from traffic and, on a much longer time scale (hours to days, rather than minutes), by net O_3 production. Under an extreme condition, if all traffic-related NO_x emissions are assumed to be NO, O_x would remain unchanged in response to lockdown-driven changes in traffic (but NO_2 would decrease, and O_3 would increase). In reality, primary NO_2 emissions from road traffic decreased during the lockdowns, so O_x should fall. Detrended O_x fell slightly at roadside and urban background sites in most of the cities (Table 1 and table S3). Detrended O_x increased at rural sites in some of the cities (table S3), which indicates an increase in net photochemical production of O_3 at some of the studied sites (28). The different pattern of changes in detrended O_3 represents a nonlinear response of O_3 formation rates to the (relative) changes in NO_x and VOC emissions, depending on the prevailing O_3 production regime at each location, but usually with a greater impact downwind of conurbation locations (29, 30).

Drivers of the response of $PM_{2.5}$ levels to the lockdown measures are more complex since both primary emissions and secondary formation contribute to $PM_{2.5}$ in ambient air. Deweathered $PM_{2.5}$ reduced after the lockdowns began at urban background sites in most of the cities, including Wuhan, Rome, New York, Los Angeles, and Delhi (fig. S2). This could be explained by (i) the expected reductions in primary emissions of $PM_{2.5}$ and its gaseous precursors (e.g., NO_2, SO_2, and VOCs) during the lockdowns and (ii) limited change in the formation rate of secondary aerosol as shown by the small variation in $PM_{2.5}$/CO ratio (fig. S5).

Deweathered $PM_{2.5}$ increased in London and Paris for an extended period (more than 3 weeks) after the lockdowns began (Fig. 5). It also increased in Beijing after the lockdown began, although for a shorter period. One possible explanation for this unexpected result is that enhanced secondary aerosol formation overwhelmed the reduced primary $PM_{2.5}$ emissions. In Chinese megacities, secondary particles typically contribute to >50% of $PM_{2.5}$ mass (31, 32). In London, secondary aerosols contribute roughly half of $PM_{2.5}$ at roadside sites, increasing to ~90% of $PM_{2.5}$ at rural sites, with the contribution lying between these values at urban background sites (33). Such contributions are even larger during pollution events (15, 16, 31). Thus, changes in $PM_{2.5}$ are often driven by variations in secondary aerosols, particularly during pollution events. In Beijing, Sun et al. (34) noted that primary aerosol decreased by 30 to 50%, while secondary inorganic aerosol and secondary organic aerosol

(SOA) increased by 60 to 110% and 52 to 175%, respectively, during the early periods of the lockdown in 2020. The fact that substantial increases in $PM_{2.5}$/PM_{10} (Paris) or $PM_{2.5}$/CO (London; fig. S5) ratios accompanied the increase in deweathered $PM_{2.5}$ (Fig. 5 and fig. S2) also supports the greater role of secondary aerosol during the study period in Paris and London. Zhao et al. (35) suggested that SOA formation depends nonlinearly on the ratio of VOCs to NO_x; reduction in NO_x emissions may lead to increased production of SOA given imbalanced emission abatement of NO_x and VOCs. Le et al. (15) indicated that multiphase chemistry and enhanced atmospheric oxidative capacity drove haze events in China during the lockdowns. Huang et al. (16) also suggested that increase in oxidative capacity during lockdown in China/Beijing caused the observed air pollution events; however, the changes in deweathered O_x levels (P_{dew}) at urban background sites are rather small: Beijing (−1.1 ± 2.0%), London (+4.2 ± 0.8%), and Paris (+2.1 ± 0.6%) (table S2).

Another possible explanation is associated with changes in long-range transport, which brings air pollutants from nonlocal sources and thus contributes to the increase in deweathered $PM_{2.5}$. In theory, the RF models should have normalized the impacts from long-range transport by including back-trajectory clusters. However, the model may not be able to perfectly reproduce secondary formation processes arising from long-range transport if there were limited cases to learn from, especially as such events tend to be episodic in nature. In this case, the model will treat pollution events arising from long-range transport as if there are higher emissions; this attribution will be retained during deweathering. This will cause uncertainties in the model. More observational data and modeling are needed to fully understand the phenomenon of increases in $PM_{2.5}$ in London, Paris, and Beijing during the lockdowns. However, it is clear that a small reduction in primary $PM_{2.5}$ emissions (e.g., from vehicular emission changes during lockdown) could be readily overwhelmed by enhanced secondary formation and/or $PM_{2.5}$ transported from more polluted regions.

In Wuhan, the deweathered $PM_{2.5}$ decreased to a small degree during the 2 weeks after the lockdown began (Fig. 5). However, the deweathered $PM_{2.5}$/CO increased during the lockdowns (fig. S5), which suggests that enhanced secondary pollution (36) offsets the benefits of the reduction in primary emissions during the first 2 weeks of the lockdown. Thereafter, the deweathered $PM_{2.5}$ did decrease more significantly (P_{dew} = −27.0 ± 18.7%). Similarly, in Beijing, the deweathered $PM_{2.5}$ decreased 2 weeks after the lockdown began, so overall P_{dew} is negative (−19.3 ± 9.6%). These results suggest that if the reduction in emissions of gaseous precursors is sufficiently large, it should eventually lead to an overall decline in $PM_{2.5}$. Such a hypothesis should be tested with chemical transport models with up-to-date emission inventories when these are available.

Implications for future air pollution control

Our results demonstrate that restrictions on economic activities, particularly traffic, brought an immediate decline in detrended NO_2 in all the studied cities. If similar levels of restriction were to have remained in place, the annual average NO_2 concentration would comply with the air quality guidelines from the World Health Organization (WHO) (i.e., 40 $\mu g\ m^{-3}$ for annual NO_2) for the cities considered under average meteorological conditions, except for a limited number of roadside sites. However, the detrended percentage decline (i.e., attributed to lockdown effects) in NO_2 is mostly below 30%. This is lower than the expected decline, partly due to the

NO_x-O_3 photochemical steady state (converting NO to NO_2), alongside seasonal effects, and partly due to the still important emissions of NO_x from stationary and mobile pollution sources. Detrended O_3 increased in most cities. This adds to the complexity of air pollution control, considering the potentially adverse impacts of O_3 on human [37, 38] and environmental health, including crop yields [39].

$PM_{2.5}$ exhibited a more complex response to the lockdown measures. $PM_{2.5}$ did not show an immediate decline to the lockdown measures except in Wuhan, Rome, and Los Angeles, even at the roadside sites. This is not too unexpected considering the relatively small contribution of road traffic to primary $PM_{2.5}$ in most of the cities studied here and a large contribution from secondary sources [16, 31]. In China, much of the recent decrease in $PM_{2.5}$ came from the reductions in residential solid fuel use and industrial activity rather than traffic emissions [18, 40]. Nevertheless, a decrease in deweathered $PM_{2.5}$ is observed in most of the cities.

In Delhi, Wuhan, and Beijing, annual average $PM_{2.5}$ concentrations are so far in exceedance of the WHO guideline (10 μg m^{-3}) that the decline is far from sufficient to bring levels into compliance. Even in those cities where the annual average $PM_{2.5}$ is close to 10 μg m^{-3}, such as London and Paris, emission reductions on the scale of the spring 2020 COVID-19 lockdown measures may still be insufficient to bring concentrations into compliance with the current WHO guidelines. In addition, the frequent $PM_{2.5}$ pollution events during the lockdowns in some cities, such as Beijing, London, and Paris, showed that actions of a magnitude similar to the lockdown measures are far from sufficient to avoid episodic pollution events in these cities. The mechanisms driving such changes have been explored in more detail by recent studies [15–17, 20].

Li *et al.* [41] suggested that aggressive reductions in NO_x and aromatic VOC emissions should be particularly effective for decreasing both $PM_{2.5}$ and O_3 in China. The huge reduction in NO_x (fig. S3) and VOCs [16] in response to the COVID-19 lockdowns did reduce $PM_{2.5}$ pollution in Beijing and Wuhan, but detrended O_3 increased substantially (Table 1), at least up until mid-May. A slower pace of VOC emission reduction, relative to that for NO_x, could risk a further increase in O_3 pollution.

In summary, emission changes associated with the early-2020 COVID-19 lockdown restrictions led to complex and substantial changes in air pollutant levels, but the changes are smaller than expected. The decrease in NO_2 will likely have benefits on public health, but the increase in O_3 would counteract at least some of this effect [37, 38]. The magnitude and even the sign of changes in $PM_{2.5}$ during the lockdowns differ significantly among the studied cities. Chemical processes of the mixed atmospheric system add complexity to efforts to abate secondary pollution (e.g., O_3 and $PM_{2.5}$) through reduction of precursor emissions (e.g., NO_x and VOCs) [42]. Future control measures will require a systematic approach toward NO_2, O_3, and $PM_{2.5}$ tailored for specific cities, taking into account both primary emissions and secondary processes, to maximize the overall benefits to air quality and human health.

MATERIALS AND METHODS
Selected cities and data
Eleven cities were selected to ensure coverage of contrasting pollution climate: Beijing and Wuhan in China, Milan and Rome in Italy, Madrid in Spain, London in United Kingdom, Paris in France, Berlin in Germany, New York and Los Angeles in the United States,

and Delhi in India. Of those, eight are capital cities. Wuhan was added because it was the first city where COVID-19 was reported and lockdown was first imposed. Milan was included because it is in northern Italy, one of the most seriously hit areas after Wuhan. In the United States, New York was the most seriously affected city, whereas Los Angeles was reported to have observed a greater decline in air pollution levels [43]. All the study cities have been significantly affected by COVID-19 and implemented stringent lockdown measures to contain the COVID-19 pandemic in early 2020. Such measures were first implemented in Wuhan from 23 January 2020 and then 2 days later in all provinces in China (including Beijing). Tightened restrictive measures were implemented from 23 January 2020 in northern Italy, 13 March 2020 in the United States, 14 March 2020 in Spain, 17 March 2020 in France, 22 March 2020 in Germany, 23 March 2020 in the United Kingdom, and 25 March 2020 in India.

Site-specific hourly concentration of six criteria pollutants ($PM_{2.5}$, PM_{10}, O_3, NO_2, CO, and SO_2) and other auxiliary pollutants (NO and NO_x) from December 2015 to May 2020 were obtained from websites of local or national environmental agency or accredited third parties (table S4). In most cases, data from multiple stations for each site type are available. The NO_2 concentrations reported from local governments, typically performed by the widely used molybdenum conversion/chemiluminescence method, may slightly overestimate true NO_2 levels due to conversion of other labile N species to NO in the convertor stage. This problem is usually small for polluted urban sites but is larger for rural sites where overestimates of 17 to 30% have been reported [44]. This is due to the conversion of NO_x from primary sources to secondary nitrogen compounds during its transport toward more rural locations. Hence, concentrations reported as NO_2 contain a small proportion of other NO_y species, and the "true" NO_2 levels would be lower than those officially reported, particularly at rural locations. We note that such uncertainties are effectively "built in" to monitor NO_2 with respect to regulatory standards. NO_x and NO data were obtained in cities where those data were publicly available. Data were usually downloaded from official sources, which are validated by the authorities. For those cities where data were not available from recognized official sources (i.e., Los Angeles and New York) at the time of access, we obtained the air quality data from the "OpenAQ" platform (https://openaq.org/). Data from Los Angeles were downloaded from the U.S. Environmental Protection Agency (USEPA) later (after the data analyses were done here), which were then compared with those from OpenAQ. We found that the site-specific data in Los Angeles from OpenAQ are highly correlated (slope = ~1, intercept = ~0) with those from USEPA. Air quality monitoring stations were selected to cover roadside, urban background, and rural sites when possible, and the site types were based on official classifications and maps. The downloaded data were screened and cleaned when necessary, following established methods [24].

The hourly temperature, relative humidity, atmospheric pressure, wind speed, and wind direction data for selected sites were obtained from the nearest meteorological observation site from the NOAA (National Oceanic and Atmospheric Administration) Integrated Surface Database (ISD) using the "worldmet" R package (https://CRAN.R-project.org/package=worldmet). In addition, hourly data for boundary layer height, total cloud cover, surface net solar radiation, and total precipitation at the selected sites were downloaded from the ERA5 reanalysis dataset (ERA5 hourly data on single levels from 1979 to present). For each site, 72-hour back trajectories at an hourly resolution were calculated using the Hybrid Single-Particle

Lagrangian Integrated Trajectory (HYSPLIT) model. The starting height was set as 100 m to ensure that the receptor was aloft but remained within the boundary layer throughout the study period. The back trajectories were then clustered into 12 clusters using the Euclidian distance by "openair" R package (https://CRAN.R-project.org/package=openair). Those clusters were used to represent the common air masses that the sites were exposed to.

Observations at the air quality stations are used for official compliance purpose. Although these stations were built to represent the specific environment of the city (i.e., roadside, urban background, and rural), there may be some variabilities in the concentrations of air pollutants at different stations of the same type. This could cause potential uncertainties in our analyses if to represent the whole city. In this study, wherever possible, we used data from multiple stations for each site type (table S4), which reduced this uncertainty. Where only one station is available for a site type, the data may be subject to more influence from local emission sources. Therefore, what we reported here should be treated in the context of the site availability (see table S4). Furthermore, we would like to emphasize that our analyses focus on the high-resolution temporal variations, and thus, the trend will be broadly representative.

RF model and weather normalization

Weather conditions change rapidly, causing variations in the concentration of air pollutants even when emissions do not change. Here, we applied a machine learning–based RF algorithm to decouple the effects of meteorological conditions. To do this, we first build an RF model for each pollutant and for each year (December to May). The RF model–based weather normalization technique was introduced in Grange et al. (12). Briefly, the RF model was built independently for each period (December 2015 to May 2016, December 2016 to May 2017, December 2017 to May 2018, December 2018 to May 2019, and December 2019 to May 2020), each pollutant, and each site type within a city. Seventy percent of the original data were randomly selected to build the model, which was then evaluated with the remainder (30%) of the dataset. Model performance for each pollutant and each time period (i.e., 2016–2020) is illustrated in fig. S6. Similar to Grange et al. (12, 13) and Vu et al. (14), the performance of the models is usually very good, much better than that of regression models (9). The weather normalization was conducted using the "rmweather" R package, available at https://cran.r-project.org/web/packages/rmweather/index.html.

In the Grange et al. (12) approach, a new dataset of input predictor features including time variables (day of the year, day of the week, and hour of the day, but not the Unix time) and meteorological parameters (wind speed, wind direction, temperature, and relative humidity) is first resampled from the original observation dataset. Vu et al. (14) modified the default method to investigate the seasonal variations in trends for comparison with trends in primary emissions, by only resampling the weather variables (not the time variables). Specifically, weather variables at a specific hour of a particular day in the input datasets were generated by randomly selecting from the historical weather data (past 30 years) at the particular hour of different dates within a 4-week period (i.e., 2 weeks before and 2 weeks after that selected date). The two methods are fit for their own purposes but were not used here because (i) Grange et al. (12) normalized the diurnal and seasonal variations of the primary emissions, which is unrealistic in the real world, and (ii) although Vu et al. (14) provided diurnal and seasonal variations of the primary emissions,

this is inappropriate in detecting short-term emission interventions because the normalized concentrations for a particular hour of a Julian day were not comparable with those from the different hour of a different Julian day, considering that they were resampled from different weather datasets, which would be affected by different seasonal weather conditions.

To address those limitations and better investigate the impacts of short-term lockdown on air quality, we applied a mixed method. We only normalized the weather data but not time variables, similar to Vu et al. (14), and resampled from the whole study period, similar to Grange et al. (12). The improved method is more suitable for tracking emission changes. The input features for the model included time variables (i.e., Unix time, Julian day, day of the week, and hour of the day), meteorological data from surface observations (i.e., temperature, relative humidity, wind speed, wind direction, and atmospheric pressure), meteorological data from ERA5 reanalysis dataset (i.e., boundary layer height, total cloud cover, surface net solar radiation, and total precipitation), and air mass clusters based on the HYSPLIT back trajectories. The day of week and air mass clusters were categorical variables, while all others were numeric. Following Vu et al. (14), the parameters for the RF models are as follows: a forest of 300 trees, n_tree = 300; the number of variables that may split at each node, mtry = 3; and the minimum size of terminal nodes, min_node_size = 3. For every weather normalization, the explanatory variables were resampled (excluding the time variables) without replacement and randomly allocated to a dependent variable observation. The 1000 predictions were then aggregated using the arithmetic mean to obtain the deweathered concentration.

REFERENCES AND NOTES

1. J. Lelieveld, A. Pozzer, U. Pöschl, M. Fnais, A. Haines, T. Münzel, Loss of life expectancy from air pollution compared to other risk factors: A worldwide perspective. *Cardiovasc. Res.* **116**, 1910–1917 (2020).
2. World Bank Group, *The Cost of Air Pollution: Strengthening the Economic Case for Action (English)* (2016); http://documents.worldbank.org/curated/en/781521473177013155/The-cost-of-air-pollution-strengthening- the-economic-case-for-action.
3. Y. Ogen, Assessing nitrogen dioxide (NO$_2$) levels as a contributing factor to coronavirus (COVID-19) fatality. *Sci. Total Environ.* **726**, 138605 (2020).
4. D. Fattorini, F. Regoli, Role of the chronic air pollution levels in the COVID-19 outbreak risk in Italy. *Environ. Pollut.* **264**, 114732 (2020).
5. C. Le Quéré, R. B. Jackson, M. W. Jones, A. J. Smith, S. Abernethy, R. M. Andrew, A. J. De-Gol, D. R. Willis, Y. Shan, J. G. Canadell, P. Friedlingstein, F. Creutzig, G. P. Peters, Temporary reduction in daily global CO$_2$ emissions during the COVID-19 forced confinement. *Nat. Clim. Chang.* **10**, 647–653 (2020).
6. S. Sharma, M. Zhang, Anshika, J. Gao, H. Zhang, S. H. Kota, Effect of restricted emissions during COVID-19 on air quality in India. *Sci. Total Environ.* **728**, 138878 (2020).
7. P. Sicard, A. D. Marco, E. Agathokleous, Z. Feng, X. Xu, E. Paoletti, J. J. D. Rodriguez, V. Calatayud, Amplified ozone pollution in cities during the COVID-19 lockdown. *Sci. Total Environ.* **735**, 139542 (2020).
8. A. Tobías, C. Carnerero, C. Reche, J. Massagué, M. Via, M. C. Minguillón, A. Alastuey, X. Querol, Changes in air quality during the lockdown in Barcelona (Spain) one month into the SARS-CoV-2 epidemic. *Sci. Total Environ.* **726**, 138540 (2020).
9. Z. S. Venter, K. Aunan, S. Chowdhury, J. Lelieveld, COVID-19 lockdowns cause global air pollution declines. *Proc. Natl. Acad. Sci.* **117**, 18984–18990 (2020).
10. R. Zhang, Y. Zhang, H. Lin, X. Feng, T.-M. Fu, Y. Wang, NO$_x$ emission reduction and recovery during COVID-19 in east China. *Atmos.* **11**, 433 (2020).
11. F. Liu, A. Page, S. A. Strode, Y. Yoshida, S. Choi, B. Zheng, L. N. Lamsal, C. Li, N. A. Krotkov, H. Eskes, R. van der A, P. Veefkind, P. F. Levelt, O. P. Hauser, J. Joiner, Abrupt decline in tropospheric nitrogen dioxide over China after the outbreak of COVID-19. *Sci. Adv.* **6**, eabc2992 (2020).

12. S. K. Grange, D. C. Carslaw, A. C. Lewis, E. Boleti, C. Hueglin, Random forest meteorological normalisation models for swiss PM$_{10}$ trend analysis. *Atmos. Chem. Phys.* **18**, 6223–6239 (2018).

13. S. K. Grange, D. C. Carslaw, Using meteorological normalisation to detect interventions in air quality time series. *Sci. Total Environ.* **653**, 578–588 (2019).

14. T. V. Vu, Z. Shi, J. Cheng, Q. Zhang, K. He, S. Wang, R. M. Harrison, Assessing the impact of clean air action on air quality trends in Beijing using a machine learning technique. *Atmos. Chem. Phys.* **19**, 11303–11314 (2019).

15. T. Le, Y. Wang, L. Liu, J. Yang, Y. L. Yung, G. Li, J. H. Seinfeld, Unexpected air pollution with marked emission reductions during the COVID-19 outbreak in China. *Science* **369**, 702–706 (2020).

16. X. Huang, A. Ding, J. Gao, B. Zheng, D. Zhou, X. Qi, R. Tang, J. Wang, C. Ren, W. Nie, V. Chi, Z. Xu, L. Chen, Y. Li, F. Che, N. Pang, H. Wang, D. Tong, W. Qin, W. Cheng, W. Liu, Q. Fu, B. Liu, F. Chai, S. J. Davis, Q. Zhang, K. He, Enhanced secondary pollution offset reduction of primary emissions during COVID-19 lockdown in China. *Natl. Sci. Rev.* 10.1093/nse/nwaa137, (2020).

17. Y. Chang, R.-J. Huang, X. Ge, X. Huang, J. Hu, Y. Duan, Z. Zou, X. Liu, M. F. Lehmann, Puzzling haze events in China during the coronavirus (COVID-19) shutdown. *Geophys. Res. Lett.* **47**, e2020GL088533 (2020).

18. Q. Zhang, Y. Zheng, D. Tong, M. Shao, X. Wang, Y. Zhang, X. Xu, J. Wang, H. He, W. Liu, Y. Ding, Y. Lei, J. Li, Z. Wang, X. Zhang, Y. Wang, J. Cheng, Y. Liu, Q. Shi, L. Yan, G. Geng, C. Hong, M. Li, F. Liu, B. Zheng, J. Cao, A. Ding, J. Gao, Q. Fu, J. Huo, B. Liu, Z. Liu, F. Yang, K. He, J. Hao, Drivers of improved PM$_{2.5}$ air quality in China from 2013 to 2017. *Proc. Natl. Acad. Sci. U.S.A.* **116**, 24463–24469 (2019).

19. G. He, Y. Pan, T. Tanaka, The short-term impacts of COVID-19 lockdown on urban air pollution in China. *Nat. Sustain.* 10.1038/s41893-020-0581-y , (2020).

20. P. Wang, K. Chen, S. Zhu, P. Wang, H. Zhang, Severe air pollution events not avoided by reduced anthropogenic activities during COVID-19 outbreak. *Res. Conserv. Recyc.* **158**, 104814 (2020).

21. Y. Zhao, K. Zhang, X. Xu, H. Shen, X. Zhu, Y. Zhang, Y. Hu, G. Shen, Substantial changes in nitrogen dioxide and ozone after excluding meteorological impacts during the COVID-19 outbreak in mainland China. *Environ. Sci. Technol. Lett.* **7**, 402–408 (2020).

22. L. Myllyvirta, H. Thieriot, *11,000 Air Pollution-Related Deaths Avoided in Europe as Coal, Oil Consumption Plummet* (CREA report, 2020).

23. A. Thorpe, R. M. Harrison, Sources and properties of non-exhaust particulate matter from road traffic: A review. *Sci. Total Environ.* **400**, 270–282 (2008).

24. J. He, S. Gong, Y. Yu, L. Yu, L. Wu, H. Mao, C. Song, S. Zhao, H. Liu, X. Li, R. Li, Air pollution characteristics and their relation to meteorological conditions during 2014–2015 in major Chinese cities. *Environ. Pollut.* **223**, 484–496 (2017).

25. X. Shi, G. P. Brasseur, The response in air quality to the reduction of Chinese economic activities during the COVID-19 outbreak. *Geophys. Res. Lett.* **47**, e2020GL088070 (2020).

26. O. Ghaffarpasand, D. C. Beddows, K. Ropkins, F. D. Pope, Real-world assessment of vehicle air pollutant emissions subset by vehicle type, fuel and EURO class: New findings from the recent UK EDAR field campaigns, and implications for emissions restricted zones. *Sci. Total Environ.* **734**, 139416 (2020).

27. C. Song, C. Ma, Y. Zhang, T. Wang, L. Wu, P. Wang, Y. Liu, Q. Li, J. Zhang, Q. Dai, C. Zou, L. Sun, H. Mao, Heavy–duty diesel vehicles dominate vehicle emissions in a tunnel study in northern China. *Sci. Total Environ.* **637**, 431–442 (2018).

28. J. H. Seinfeld, S. N. Pandis, *Atmospheric Chemistry and Physics: From Air Pollution to Climate Change* (John Wiley & Sons, 2016).

29. T. Wang, L. Xue, P. Brimblecombe, Y. F. Lam, L. Li, L. Zhang, Ozone pollution in China: A review of concentrations, meteorological influences, chemical precursors, and effects. *Sci. Total Environ.* **575**, 1582–1596 (2017).

30. K. Li, D. J. Jacob, H. Liao, L. Shen, Q. Zhang, K. H. Bates, Anthropogenic drivers of 2013–2017 trends in summer surface ozone in China. *Proc. Natl. Acad. Sci. U.S.A.* **116**, 422–427 (2019).

31. R.-J. Huang, Y. Zhang, C. Bozzetti, K.-F. Ho, J.-J. Cao, Y. Han, K. R. Daellenbach, J. G. Slowik, S. M. Platt, F. Canonaco, P. Zotter, R. Wolf, S. M. Pieber, E. A. Bruns, M. Crippa, G. Ciarelli, A. Piazzalunga, M. Schwikowski, G. Abbaszade, J. Schnelle-Kreis, R. Zimmermann, Z. An, S. Szidat, U. Baltensperger, I. E. Haddad, A. S. H. Prévôt, High secondary aerosol contribution to particulate pollution during haze events in China. *Nature* **514**, 218–222 (2014).

32. C.-S. Liang, F.-K. Duan, K.-B. He, Y.-L. Ma, Review on recent progress in observations, source identifications and countermeasures of PM$_{2.5}$. *Environ. Int.* **86**, 150–170 (2016).

33. G. McFiggans, M. R. Alfarra, J. D. Allan, H. Coe, J. F. Hamilton, R. M. Harrison, M. E. Jenkin, A. C. Lewis, S. J. Moller, D. Topping, P. I. Williams, *A Review of the State-Of-The-Science Relating to Secondary Particulate Matter of Relevance to the Composition of the UK Atmosphere: Full Technical Report to Defra, Project AQ0732* (Research Report, Defra, 2015).

34. Y. Sun, L. Lei, W. Zhou, C. Chen, Y. He, J. Sun, Z. Li, W. Xu, Q. Wang, D. Ji, P. Fu, Z. Wang, D. R. Worsnop, A chemical cocktail during the COVID-19 outbreak in Beijing, China:

Insights from six-year aerosol particle composition measurements during the Chinese new year holiday. *Sci. Total Environ.* **742**, 140739 (2020).

35. Y. Zhao, R. Saleh, G. Saliba, A. A. Presto, T. D. Gordon, G. T. Drozd, A. H. Goldstein, N. M. Donahue, A. L. Robinson, Reducing secondary organic aerosol formation from gasoline vehicle exhaust. *Proc. Natl. Acad. Sci. U.S.A.* **114**, 6984–6989 (2017).

36. H. Zheng, S. Kong, N. Chen, Y. Yan, D. Liu, B. Zhu, K. Xu, W. Cao, Q. Ding, B. Lan, Z. Zhang, M. Zheng, Z. Fan, Y. Cheng, S. Zheng, L. Yao, Y. Bai, T. Zhao, S. Qi, Significant changes in the chemical compositions and sources of PM$_{2.5}$ in Wuhan since the city lockdown as COVID-19. *Sci. Total Environ.* **739**, 140000 (2020).

37. Q. Di, Y. Wang, A. Zanobetti, Y. Wang, P. Koutrakis, C. Choirat, F. Dominici, J. D. Schwartz, Air pollution and mortality in the medicare population. *N. Engl. J. Med.* **376**, 2513–2522 (2017).

38. COMEAP, *Associations of long-term average concentrations of nitrogen dioxide with mortality, Committee on the Medical Effects of Air Pollutants report, Public Health England* (2018); www.gov.uk/government/publications/nitrogen-dioxide-effects-on-mortality.

39. M. R. Ashmore, Assessing the future global impacts of ozone on vegetation. *Plant Cell Environ.* **28**, 949–964 (2005).

40. B. Zhao, H. Zheng, S. Wang, K. R. Smith, X. Lu, K. Aunan, Y. Gu, Y. Wang, D. Ding, J. Xing, V. Fu, X. Yang, K.-N. Liou, J. Hao, Change in household fuels dominates the decrease in PM$_{2.5}$ exposure and premature mortality in China in 2005–2015. *Proc. Natl. Acad. Sci. U.S.A.* **115**, 12401–12406 (2018).

41. K. Li, D. J. Jacob, H. Liao, J. Zhu, V. Shah, L. Shen, K. H. Bates, Q. Zhang, S. Zhai, A two-pollutant strategy for improving ozone and particulate air quality in China. *Nat. Geosci.* **12**, 906–910 (2019).

42. J. H. Kroll, C. L. Heald, C. D. Cappa, D. K. Farmer, J. L. Fry, J. G. Murphy, A. L. Steiner, The complex chemical effects of COVID-19 shutdowns on air quality. *Nat. Chem.* **12**, 777–779 (2020).

43. Q. Schiermeier, Why pollution is plummeting in some cities-but not others. *Nature* **580**, 313 (2020).

44. M. Steinbacher, C. Zellweger, B. Schwarzenbach, S. Bugmann, B. Buchmann, C. Ordóñez, A. S. H. Prevot, C. Hueglin, Nitrogen oxide measurements at rural sites in Switzerland: Bias of conventional measurement techniques. *J. Geophys. Res. Atmos.* **112**, D11307 (2007).

Citation: Z. Shi, C. Song, B. Liu, G. Lu, J. Xu, T. Van Vu, R. J. R. Elliott, W. Li, W. J. Bloss, R. M. Harrison, Abrupt but smaller than expected changes in surface air quality attributable to COVID-19 lockdowns. *Sci. Adv.* **7**, eabd6696 (2021).